BIOSYSTEMS ENGINEERING 164 (2017) 49–67

Available online at www.sciencedirect.com

ScienceDirect

journal homepage: www.elsevier.com/locate/issn/15375110

Review

Close range hyperspectral imaging of plants: A review

Puneet Mishra [a,d,*], *Mohd Shahrimie Mohd Asaari* [a], *Ana Herrero-Langreo* [b], *Santosh Lohumi* [c], *Belén Diezma* [d], *Paul Scheunders* [a]

[a] *Vision Lab, Department of Physics, Campus Drie Eiken, University of Antwerp, Edegemsesteenweg 200-240, 2610 Antwerp, Belgium*

[b] *Irstea, UMR ITAP, 361 Rue J.F. Breton, 34196 Montpellier Cedex 5, France*

[c] *Department of Biosystems Machinery Engineering, College of Agricultural and Life Science, Chungnam National University, 99 Daehak-ro, Yuseong-gu, Daejeon 305-764, South Korea*

[d] *LPF-TAGRALIA, School of Engineering for Agriculture, Food and Biosystems, Technical University of Madrid, 28040 Madrid, Spain*

ARTICLE INFO

Article history:
Received 20 March 2017
Received in revised form
6 September 2017
Accepted 24 September 2017
Published online 23 October 2017

Keywords:
Plant traits
Phenotyping
Pigments
Non-destructive
Imaging spectroscopy

The increasing need to develop a rapid understanding of plant functional dynamics has led to the employment of sensor technology for non-destructive assessment of plants. Hyperspectral Imaging (HSI) being an integration of two modalities, imaging and point spectroscopy, is nowadays emerging as a potential tool for rapid, non-destructive and automated close range assessment of plants functional dynamics both in terms of structure and physiology.

Firstly, this paper presents an overview of some basic concepts of close range HSI on plants, concerning the plant–light interaction, instrumental setup, and spectral data analysis. Furthermore, the work reviews recent advances of HSI for plant related studies under controlled experimental conditions as well as in natural agricultural settings. Applications are discussed on foliar content estimation, variety identification, growth monitoring, stress and disease-related studies, phenotyping and adoption of HSI in high-throughput phenotyping platforms (HTPPs).

Close range HSI is a challenging task and suffers from technical complexities related to external factors (e.g. illumination effects) as well as plant-related factors (e.g. complex plant geometry). The paper finally discusses some of the technical challenges related to the implementation of HSI in the close range assessment of plant traits.

1. Introduction

To increase the agriculture productivity, it is important to develop high-yielding crops which can adapt to future climatic conditions (Furbank & Tester, 2011). Moreover, the assessment of existing and to be developed high-yielding crop plants is crucial to understand how the detrimental effects of surrounding environment limit their growth and yield, further

* *Corresponding author*. Pure and Applied Chemistry, Thomas Graham Building, University of Strathclyde, 295 Cathedral St, Glasgow G1 1XL, United Kingdom.
E-mail address: puneet.mishra@alumnos.upm.es (P. Mishra).

https://doi.org/10.1016/j.biosystemseng.2017.09.009
1537-5110/

Nomenclature

(x,y)	Spatial coordinate of HSI
3D	Three dimensional
AMB	Apple marssonina blotch
ANN	Artificial neural network
BLR	Binary logistic regression
deg C	Celsius
C–O	Carbon and oxygen bond
CCD	Charge coupled device
CLS	Cercospora leaf spot
CMOS	Complementary metal-oxide-semiconductor
CSIRO	Commonwealth scientific and industrial research organisation
e.g.	Example
ELM	Extended learning machine
EM	Electromagnetic
EMR	Electromagnetic radiation
g cm^{-2}	gram per square centimetre
GA-PLS	Genetic algorithm partial least square
g kg^{-1}	gram per kilogram
g m^{-2}	gram per square metre
HPLC	High performance liquid chromatography
HSI	Hyperspectral imaging
HTPPs	High-throughput phenotyping platforms
I_{dark}	Dark reference
I_R	Reflectance
I_{raw}	Raw image
I_{white}	White reference
ICA	Independent component analysis
InGaAs	Indium gallium arsenide
λ	wavelength
LDA	Linear discriminant analysis
LED	Light emitting diode
mg g^{-1}	milligram per gram
MLR	Multiple linear regression
MSC	Multiplicative scatter correction
N–H	Nitrogen hydrogen bond
NIR	Near-infrared
nm	nanometre
O–H	Oxygen hydrogen bond
O_3	Ozone
PCA	Principal component analysis
PLS-LDA	Partial least square linear discriminant analysis
PLSR	Partial least square regression
POD	Per-oxidase
PSI	Photon system instruments
R^2	Correlation coefficient
R692/R530	Ratio of 692 and 530 wavebands
R692/R732	Ratio of 692 and 732 wavebands
R702/R718	Ratio of 702 and 718 wavebands
RGB	Red green blue
RMSE	Root mean squared error
ROI	Region of interest
SAM	Spectral angle mapper
SiVM	Simplex volume maximisation
SNV	Standard normal variate
SVM	Support vector machine
SVR	Support vector regression
SWIR	Short-wave infrared
TMV	Tobacco mosaic virus
UV	Ultraviolet
VIB	Vlaams Instituut voor Biotechnologie
VIS	Visible

supporting the development of optimal plant varieties. Traditional methods used for plant assessment are still time-consuming, labour intensive and destructive in nature (Busemeyer et al., 2013).

The need for fast, non-destructive and high throughput alternative technologies for plant assessment has lead to the development of new and the re-use of different existing sensor technologies from various scientific domains (Li, Zhang, & Huang, 2014). One such emerging sensor technology for non-destructive, rapid and automated assessment of plants is the hyperspectral imaging (HSI) (Matsuda, Tanaka, Fujita, & Iba, 2012). The application of HSI can be found in diverse domains of research such as remote sensing (Blackburn, 2007), foods (Mishra et al., 2015, 2016; Wu & Sun, 2013), microbiology (Gowen, Feng, Gaston, & Valdramidis, 2015) and pharmaceutical sciences (Gendrin, Roggo, & Collet, 2008). In particular, in remote sensing, vegetation monitoring has been studied using HSI for many years (Blackburn, 2007), and has motivated the use of HSI for exploring plants at close range.

A HSI system integrates a spectrograph that records reflectance in a wide range of the spectrum, including the ultraviolet (UV), visible (VIS) and near-infrared (NIR) into a digital sensor (Bock, Poole, Parker, & Gottwald, 2010). Data is generated in the form of a 3D spatial map of spectral variation: the first two dimensions provide the spatial information and a third dimension accounts for the spectral information. Being an integration of imaging and conventional spectroscopy, HSI can obtain complementary information from both domains. While point spectroscopy gathers information to understand the physiology of the plants (Montes, Melchinger, & Reif, 2007), the information from imaging technology is used to understand the structural dynamics (Apelt, Breuer, Nikoloski, Stitt, & Kragler, 2015; Bucksch et al., 2014; Dhondt et al., 2014). In combination, HSI has the potential to extract integrated spatial and spectral information related to the plant's functional dynamics regarding both structure and physiology (Bergsträsser et al., 2015; Kuska et al., 2015; Mahlein, Oerke, Steiner, & Dehne, 2012; Rascher et al., 2011; Ustin & Gamon, 2010).

Various emerging applications of HSI related to plants biochemistry estimation (Vigneau, Ecarnot, Rabatel, & Roumet, 2011), stress detection (Rumpf et al., 2010; Mahlein, Steiner, Dehne, & Oerke, 2010, 2013), species identification (Kumar, Skidmore, & Mutanga, 2010) and Phenotyping (Leucker et al., 2017; Wahabzada et al., 2016) have gained the interest of plant biologists and agronomist all over the globe, covering the need for a fast, non-destructive and visually

interpretable technology (Fiorani, Rascher, Jahnke, & Schurr, 2012; Rascher et al., 2011). Furthermore, HSI has been increasingly integrated with high-throughput phenotyping platforms (HTPPs) for controlled and automated assessment of plants (Busemeyer et al., 2013). HTPPs perform qualitative and quantitative determination of functional plant traits, such as plant growth and biomass yield, resulting from the interaction of the genetic characteristics of the plant with surrounding controlled environmental conditions (Furbank & Tester, 2011). These functional traits are reflected into different regions of the reflectance spectrum and can be estimated through HSI.

The HSI can be used to image the complete plants, as is required in a monitoring experiment, as well as to image plucked leaves from the plants to perform quantitative or qualitative analysis of interest. Individual plant pixels captured by HSI provide spectral information related to the chemical composition of the plant, i.e. its physiological status (Behmann, Mahlein, Rumpf, Römer, & Plümer, 2015). To understand the effects of artificial or natural environmental factors, the plant spectra can be explored and used for model development. For example, in the case of stress related studies, stress resulting from a drought induces degradation of the leaf chlorophyll content leading to an increase in reflectance over the whole VIS spectrum (400–700 nm). Similar information generated by HSI can be used for identification, quantification and spatial representation of nutrient deficiencies, diseases, and drought under controlled experiments in a greenhouse or under uncontrolled conditions in an agriculture field (Sankaran, Mishra, Ehsani, & Davis, 2010).

The aim of the paper is to provide the reader with an overview of the principles, instrumentation and data handling of close range HSI of plants, followed by a review of recent applications of plant assessment using HSI. Finally, the major challenges associated with the implementation of close range HSI for plants are discussed, and the paper is concluded with some future directions. All the applications reviewed in the paper were studies performed after the year 2000 and were selected from six different domains related to exploration of plants, i.e. foliar biochemistry estimation, leaf monitoring, species identification, stress detection, phenotyping and HTPPs.

2. Interaction of plants with light

The interaction of light (electromagnetic radiation (EMR)) with plants differs according to the light frequencies. Since the leaves are mainly responsible for the photosynthetic activity, the interaction of light with the leaves is of particular interest (Jacquemoud & Ustin, 2001). For green leaves, the relevant regions of EMR are the VIS region (400–700 nm), responsible for absorption of light by photosynthetic pigments; the NIR (700–1100 nm), dominated by absorption by dry matter; and the short-wave infrared (SWIR) (1100–2500 nm), where absorption by water takes place.

When light enters the leaf surface, its EM field interacts with the localised EM field of atoms within the surface. The optical properties of leaves and the characteristics of the incident light determine how the light gets affected. Typically, light can interact with leaves in the following ways: reflection, scattering, absorption and transmission. Commonly, the first interaction takes place at the surface, where part of the light is reflected back as illustrated in Fig. 1(a). Upon entering just beneath the surface level, light is scattered (Fig. 1(b)). In scattering, the light ray interacts with the leaves structures which cause irregularities (deflections) in its propagation Chen, Morris, and Martin (2006). When these abnormalities

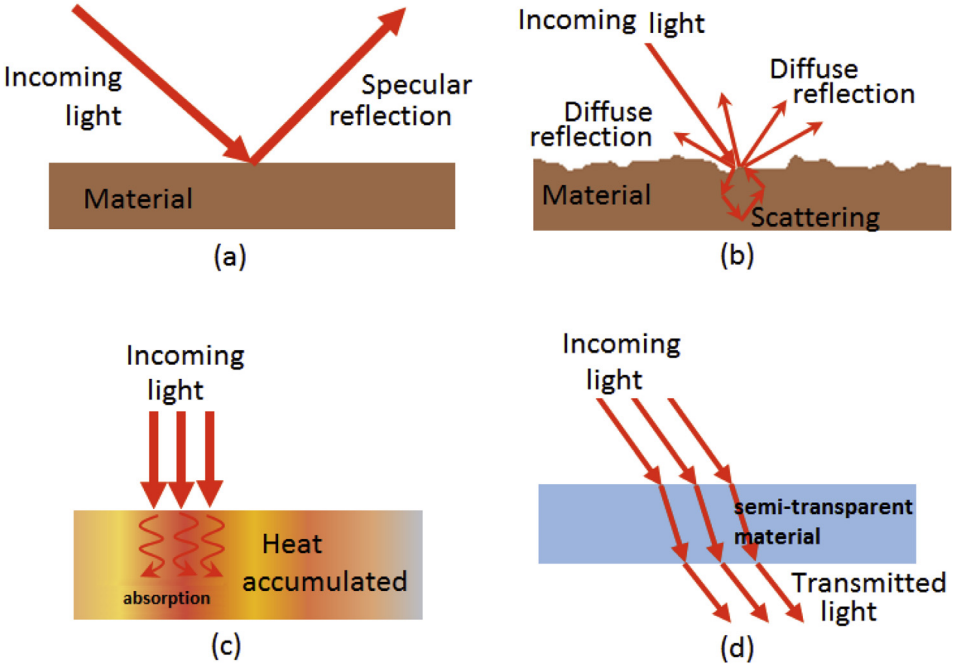

Fig. 1 – Interaction of light with leaf. (a) specular reflection, (b) diffuse reflection, (c) light absorption and (d) light transmission.

are considered to be random and dense enough, the average of their individual effects leads to a common physical phenomenon called diffuse reflection. In absorption, illustrated in Fig. 1(c), the photon transfers all its energy to an electron in the absorbing material. The electron is excited to a higher energy state in the electron configuration and moved to the neighbouring atoms in the form of thermal energy. In transmission, the atoms take in the wave, vibrate briefly, transferring the vibrations throughout the body of the leaves, and then re-emit the wave as light out the other end (Fig. 1(d)).

The reflectance characteristic of a plant results from the biochemical compounds present in the leaves, and the physical characteristics of leaves such as the fraction of air spaces and air–water interfaces. The biochemical components of leaves are mainly made up of four elements: hydrogen, carbon, oxygen and nitrogen. The resulting reflectance is caused by the interaction of light with C–O, O–H, C–H, and N–H bonds, leading to vibrations, overtones, and combinations of vibrations (Kokaly & Clark, 1999). The interaction of light within leaves changes the spin and angular momentum of the electrons leading to transitions between electrons in atoms and vibrational–rotational modes in polyatomic molecules (Jacquemoud & Baret, 1990).

A typical reflectance spectrum (400–2500 nm) arising from a green leaf can be seen in Fig. 2. The spectrum is simulated with the help of an online database on leaf optical properties (http://opticleaf.ipgp.fr/). The parameters used to perform the simulation were leaf structure parameter (1.2), chlorophyll content (30 g cm^{-2}), carotenoid content (10 g cm^{-2}), brown pigments (1), equivalent water thickness (0.015 cm) and leaf mass per unit area (0.009 g cm^{-2}). Typically, for the green leaves, the visible region (400–700 nm) is dominated by absorption of light by photosynthetic pigments; the near infrared (700–1100 nm) by dry matter; and the SWIR (1100–2500 nm) by water. Leaves have a higher reflectance in the NIR as compared to the VIS range. The spectral reflectance of healthy green leaves is particularly low in the VIS range because there is strong absorption by leaf pigments (mainly chlorophyll), with a characteristic peak reflectance at the green wavelength band. As a consequence, the healthy plants appear greener. At around 700 nm, the reflectance rises sharply to a value of around 40–50% for most plants. This high reflectance is due to scattering of a large portion of the light with the leaf cell structure, mainly within the mesophyll.

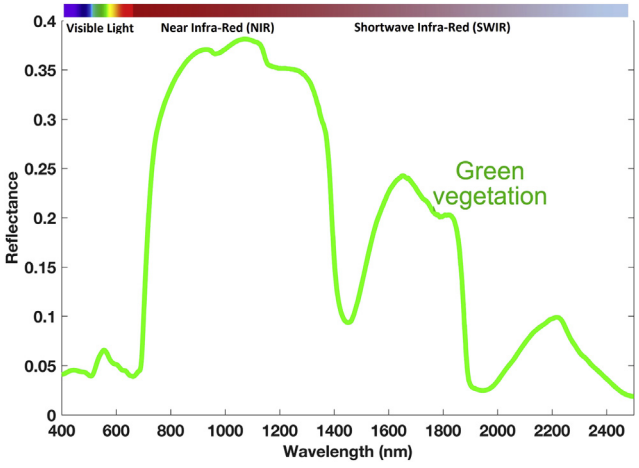

Fig. 2 – Reflectance spectra signature of green vegetation. (For interpretation of the references to colour in this figure legend, the reader is referred to the web version of this article.)

Chlorophylls, carotenoids and anthocyanin are mostly responsible for the spectral profile in the visible range. These pigments are usually present in different amounts and are closely related to the photosynthetic activity of the plants (Feret et al., 2008). Any variability in the surrounding environment such as air pollution, accumulation of heavy metals, viral attacks, insect attacks or stress, e.g. resulting from water deficiency can cause a change in the normal photosynthetic activities of the plants leading to a change in the concentrations of the pigments. For example, the accumulation of carotenoids and anthocyanin in the leaves is considered to be a natural defensive mechanism of plants in response to various kinds of environmental stresses (Springob, Nakajima, Yamazaki, & Saito, 2003). Such relationships between cause and consequence can be used to study the biochemistry of plants and to perform controlled experiments as in plant phenotyping.

3. Hyperspectral imaging

3.1. *Imaging sensor*

A HSI setup consists four main parts: the light source, the objective lenses, the imaging spectrograph and the area detector. The selection of the light source is crucial to ensure good performance and reliability of any optical inspection system. Typically, halogen lamps are most widely used in HSI systems for indoor applications related to plants (Behmann, Steinrücken, & Plümer, 2014; Matsuda et al., 2012; Yu et al., 2014). Halogen lamps are broadband illumination sources covering the visible and NIR regions. Halogen light sources provide a very stable smooth and monotonic spectrum. Whenever high power, small wavelength range illumination is needed (Mahlein et al., 2015), light emitting diodes (LED) can be a good alternative to halogen lighting.

Similar as in conventional imaging, objective lenses are used to obtain an appropriate spatial resolution in HSI systems. A key element for choosing an appropriate objective lens is based on its capability to focus incoming light from a small region (the Field of View) onto a given detector element, forming a pixel in the resulting image. Two major variables for deciding on objective lenses are the size of the optical entrance aperture relative to the wavelength and the size of the detector element relative to the optical lenses of the HSI system Edelman, Gaston, Van Leeuwen, Cullen, and Aalders (2012).

As the light passes through the objective lenses, it enters a spectrograph. A spectrograph is an instrument used to split or disperse light into distinct wavelengths. In an imaging spectrograph, diffraction gratings are used for wavelength dispersion. Diffraction gratings are optical elements consisting of a series of equally spaced grooves with a precise pattern of microscopic periodic structures. Diffraction gratings can be either reflective or transmissive. A reflection grating has its

corrugated surface coated with a metal to enhance reflectivity. In transmission gratings, incident light is diffracted upon transmission through the grating. Most commercial spectrometers use reflection gratings as they provide higher image quality and are free of higher-order aberrations, have low distortion, a low f-number, and a large field size (Bannon & Thomas, 2005). As light transmits through or reflects off a grating, the grooves diffract and further disperse the light into its component wavelengths.

Finally, the dispersed light is projected onto a detector which converts the photons into electrical signals that a computer interprets to measure the strength of different wavelengths in term of intensity values. Charge coupled device (CCD) and complementary metal-oxide-semiconductor (CMOS) are two major types of solid state area detectors used as image sensors. A CCD sensor consists of a mass of photodiodes called pixels that are made of light-sensitive materials such as Silicon (Si) and Indium Gallium Arsenide (InGaAs). The pixels in the CCD sensor can be arranged in 1-D or 2-D arrays, resulting in line and area detectors respectively (Qin, 2010, pp. 133–172). CCD sensors produce high-quality, low noise and large pixels, which make them a popular choice to be used in HSI system. CMOS sensors have specific advantages over the CCD such as high speed, low cost, low power consumption and small size for system integration (Litwiller, 2005).

The image acquisition system can be optimised by integrating a computer controlled intelligent automated system as shown in Fig. 3. A motorised platform can be used for automating the experiments, as required for HTPPs.

3.2. *Hypercube data*

HSI is relatively new technology that involves the integration of two acquisition modes: spectroscopy and imaging (Amigo, Babamoradi, & Elcoroaristizabal, 2015; Bock, Parker, Cook, & Gottwald, 2008; Gowen, O'Donnell, Cullen, Downey, & Frias, 2007). It simultaneously measures spectral signatures and spatial information from a test material within the sensor field of view. Spectral information is collected at each point and mapped onto every pixel in a rectangular spatial arrangement. The output of HS data is a series of narrow band sub-images arranged across the reflectance spectrum, forming a 3-D cube. As an example, the HSI cube of a green leaf acquired in reflectance mode is shown in Fig. 4(a). The 3-D cube data involves two spatial dimensions (x, y) and one spectral dimension (λ). The image element of this hypercube $I(x, y, \lambda)$ is termed as a voxel". The intensity values of a particular pixel characterise its unique spectral fingerprint as shown in Fig. 4(b).

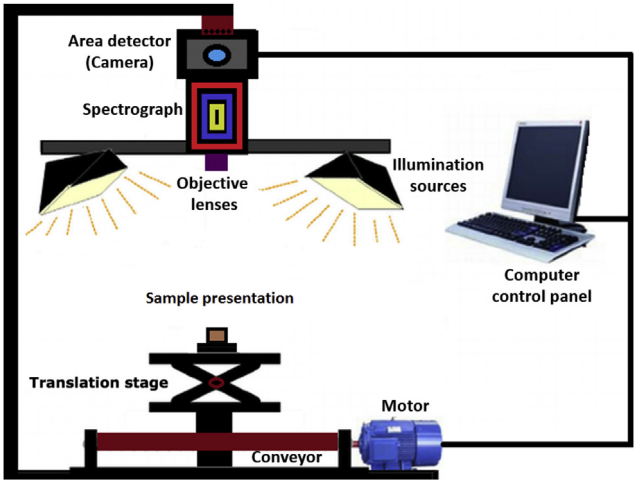

Fig. 3 – Hyperspectral imaging in a close-range setup integrated with an advanced computer control system (Inspired from Phenovision http://www.psb.ugent.be/phenotyping/phenovision).

The 3-D hypercube data can be acquired through four basic techniques: point scanning (whisk-broom), line scanning (push-broom), area scanning (spectral scanning) and snapshot (non-scanning) (Gowen et al., 2007). In a point scanning system (Fig. 5(a)), the complete spectrum is sequentially acquired for each single point. The whole scene is scanned by moving either the detector or the sample across both spatial directions (x, y) to obtain the complete hypercube. Point scanning has two primary disadvantages: a high time consumption in positioning the sample and the need of stabilised hardware mounts to ensure accurate image reconstruction. The second approach is known as the line scanning or push-broom method (Fig. 5(b)). In this method, the spectra of a whole line of pixels are acquired simultaneously. The light that enters the objective lens is dispersed onto a 2D-CCD detector. To acquire the complete hypercube, the sample is scanned across the sample surface in a direction perpendicular to the imaging line. Since this requires a relative movement between the sample and the imaging platform, an advanced pointing device is needed to reduce the effects of motion artefacts. In spectral scanning (Fig. 5(c)), full scene information from a fixed field of view is acquired as a 2-D monochromatic image at a single wavelength at a time, using band pass filters, until a full spectral hypercube is obtained. The primary disadvantage of spectral scanning is the occurrence of spectral smearing in the case of within-scene movement. Nonetheless, as an advantage, it allows to pick and choose spectral bands, providing a direct representation of the two spatial dimensions of the scene. Finally, snapshot methods (Fig. 5(d)) record both spatial and spectral information simultaneously. Primary advantages are shorter acquisition times and prevention of motion artefacts. However, such systems are still in an early stage of development and cover only a limited range of spatial and spectral resolutions.

3.3. *Processing of hypercube data*

3.3.1. *Calibration*

The raw image collected by HSI not only acquires information about the plants but also reflects the influence of nuisance signals coming from illumination effects, the detector sensitivity and the transmission properties of the optics (Geladi, Burger, & Lestander, 2004). The effects of this influence are a function of wavelength, but may also be presented as variations in the spatial domain. Spectral calibration is required to compensate for these effects. In spectral calibration, the raw intensity image is calibrated with black and white reference images. The black image is acquired when the light source and

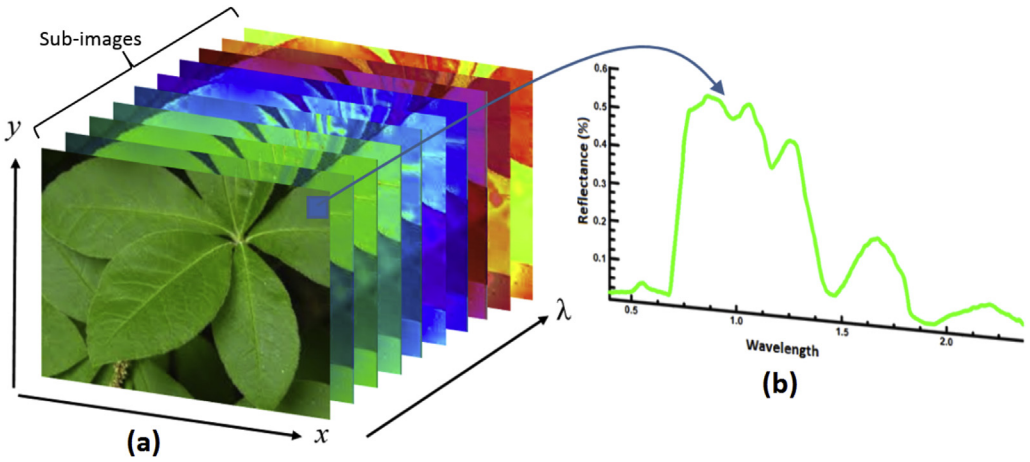

Fig. 4 – Example of hyperspectral image acquired from a green leaf. (a) Stack of narrow band sub-images forming a 3-D hypercube; (b) reflectance spectrum of a particular pixel. (For interpretation of the references to colour in this figure legend, the reader is referred to the web version of this article.)

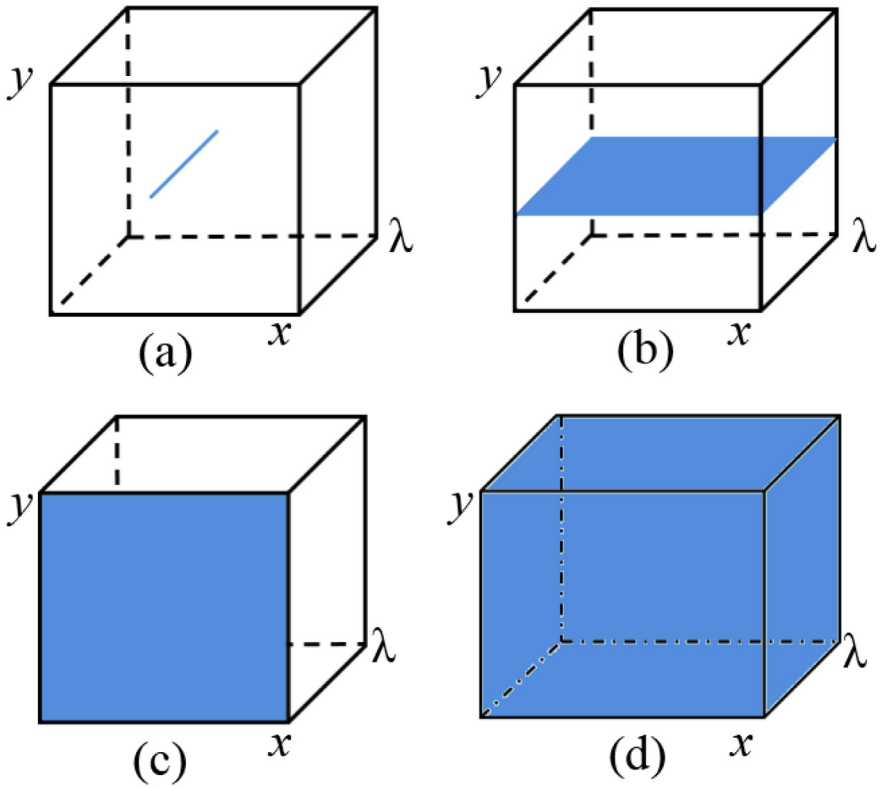

Fig. 5 – Hyperspectral image acquisition mode. (a) point scanning; (b) line scanning; (c) area scanning; (d) snapshot method.

the camera shutter are completely turned off. The white reference image is obtained by imaging a white surface board from materials such as spectralon or Teflon, which has a uniform, stable and high reflectance surface. These two reference images can be used to correct the raw images by using the following equation:

$$I_R = \frac{I_{raw} - I_{dark}}{I_{white} - I_{dark}} \quad (1)$$

where, I_R is the calibrated reflectance image, I_{raw} is the raw intensity image measured from the test sample, I_{dark} the intensity of the black reference, and I_{white} is the white reference intensity.

3.3.2. *Pre-treatment*

Another issue that needs to be taken into account before proceeding with the further analysis is tracking and handling of noises in the reflectance image (Burger, 2009). Noises can be

present in the image as dead pixels and spikes. Dead pixels are caused by abnormalities in the detector leading to permanent black pixels. They can exist in different patterns ranging from a single pixel, a group or even a complete line of pixels. A spike appears as a sharp rise followed by a sharp decline in the spectrum of a particular pixel. The best way to handle dead pixels and spikes is to substitute their values with an interpolated value, either in spectral or in the spatial domain. In spectral domain, the most common way of interpolation is by applying a signal smoothing algorithm such as a moving average (Guiñón, Ortega, García-Antón, & Pérez-Herranz, 2007) or a Savitzky–Golay filter (Luo, Ying, & Bai, 2005). Interpolation in spatial domain can be done by applying an average or median filter.

Spectral calibration and smoothing are not sufficient to correct for variations due to the complex geometry of the sample (i.e. spherical, elliptic, curvy, wavy or irregular surface and shapes). Particularly for close range HSI, variability arising from these complex geometrical patterns is very prevailing and can overlay desired spectral information of the test sample. This unwanted variability usually introduces specular reflection and multiplicative and additive effects (due to the disparity in distance and orientation towards the illumination source), baseline shift and scattering effects (due to surface heterogeneity). There are numerous pre-pretreatment techniques that can be applied to deal with these variations, for example normalisation (Polder & van der Heijden, 2010), mean centring (Jay, Hadoux, Gorretta, & Rabatel, 2014), Savitzky Golay smoothing (Savitzky & Golay, 1964), standard normal variate (SNV; Barnes, Dhanoa, & Lister, 1989) and multiplicative scatter correction (MSC; Burger, 2006). The normalisation and mean centring techniques usually are used to remove scaling and additive effects. Derivative techniques are often used for eliminating a constant offset or linear baseline shift.

SNV combines centring and normalising by a row oriented transformation to centre and scale individual spectra into a common range of zero mean and unit standard deviation. MSC is often used to compensate for additive or multiplicative effects. MSC and SNV are both competent to reduce the spectral variability from scattering and baseline shifts. However, the use of MSC requires a reference spectrum, whereas SNV works independently for every spectrum.

3.3.3. *Segmentation*

Segmentation splits the image into multiple distinct regions based on their similarity concerning some spatial or spectral properties, to reduce the image complexity for further analysis (Wu & Sun, 2013). The output from this operation can be used as a mask for the formation of a region of interest (ROI) for further spectral and spatial information extraction (ElMasry, Wang, & Vigneault, 2009). There are some image segmentation algorithms which can be applied based on the threshold, clustering, morphological operations, edge or contour detection and watershed transformation (Gonzalez, Woods, & Eddins, 2009). All these techniques can adequately perform segmentation on a single wavelength image or a monochromatic image with a scalar intensity value (spatial properties). Typically, the easiest way to perform image segmentation in the spatial domain is by using threshold methods. In this method, each pixel in an image is set to a black pixel if the pixel value is less than a predefined threshold value or a white pixel if its intensity is larger than that threshold. The output of this segmentation is a binary image which is used to create a mask to focus on the main objects to be analysed. Instead of using spatial properties, segmentation can also be performed based or spectral properties. In this approach, every pixel in an image is presented as a vector of intensity values. Spectral segmentation is considered a higher-level analysis and requires more computational time than the spatial segmentations techniques. It usually integrates several segmentation algorithms into a single process. This approach has been successfully used in applications to discriminate symptoms caused by *Heterodera schachtii* and *Rhizoctonia solani* on sugar beet (Hillnhütter, Mahlein, Sikora, & Oerke, 2012) and for early stress detection in crop plants (Behmann, Steinrücken, et al., 2014), where integration of *k*-Means clustering with vegetation index thresholds is used to segment plants from background objects.

3.3.4. *Spectral analysis*

To extract interpretable information from the complex dataset contained in the HSI hypercube, the spectra need to be analysed. As discussed in previous sections, the spectral profile can be related both to chemical and physical properties. In the case of HSI, the information is usually mixed in both the spectral and in the spatial dimensions: chemical properties are rarely related to single wavelengths and a pixel usually contains mixed information of more than one compound (Amigo et al., 2015). The spatial distribution of the spectra can be used to identify objects and their attributes such as shape, size, texture, etc. (Amigo et al., 2015; Amigo, Marti, & Gowen, 2013; Hernández-Sánchez, Moreda, Herre-ro Langreo, & Melado-Herreros, 2016; de Juan, Maeder, Hancewicz, Duponchel, & Tauler, 2009, pp. 65–109). As a consequence, HSI is inherently linked to multivariate data analysis (Amigo et al., 2013) and the particular spectral analysis to be applied depends on the objective as well as on the chemical properties of the sample (de Juan et al., 2009, pp. 65–109). For studying plant traits at close range distance, spectral analysis is applied both based on discrete single wavelengths (Multispectral Image Analysis) and on the complete spectral profiles (HSI analysis). A common multispectral approach is the calculation of vegetation indices which is typically used in satellite based remote sensing of vegetation (Jensen, 2007).

In an another approach, a number of latent variables or features are defined based on statistical measures, such as maximum variance, orthogonality etc., to represent the useful information over the entire spectrum. However, a high-dimensional feature vector often contains redundant information, where in most cases the relevant information can be represented in a few key latent variables (Behmann et al., 2015). Reducing a number of variables is an important step for high-dimensional data analysis to avoid the Hughes phenomenon, which leads to a decrease in predictive power when increasing the number of variables (Hughes, 1968).

Defining the features of interest can be done in two ways: feature selection or feature extraction. In feature selection, the number of features is reduced by selecting a subset of the most discriminating features which minimise the reconstruction error rate. There are several techniques of feature selection available in the literature, which can be categorised

as the filter, wrapper or embedded methods (Saeys, Inza, & Larrañaga, 2007). In feature extraction, a new set of features is created by transforming the data into a new feature space. A common feature extraction technique, used on HS data, is based on a linear combination of image band such as in principle component analysis (PCA; Tsai, Lin, & Yoshino, 2007) or independent component analysis (ICA; Xiaobo et al., 2010).

According to the type of outcome required, HSI modelling methods can further be categorised into classification (qualitative outcome) and regression methods (for quantitative estimations). In classification, the main objective is to automatically identify or categorise the pixels containing spectrally distinct characteristics based on feature representations specified by the user. Classification can be done in an unsupervised or supervised fashion. In unsupervised classification, the aim is to infer a function to describe the hidden structure of the data without prior knowledge of the class membership of the data. In the supervised case, the membership classes are defined and functions are modelled based on the given class information.

Typical unsupervised algorithms for the analysis of HSI, that were used in recent work include *k*-means clustering (Behmann, Steinrücken, et al., 2014) and simplex volume maximisation (SiVM; Römer et al., 2012). Common supervised classification methods used for analysis of HSI include support vector machines (SVM; Rumpf et al., 2010), partial least squares-linear discriminant analysis (PLS-LDA; Hadoux, Gorretta, & Rabatel, 2012), spectral angle mapper (SAM; Oerke, Herzog, & Toepfer, 2016), artificial neural networks (ANN; Arens et al., 2016) and linear discriminant analysis (LDA; Zhu, Cen, Zhang, & He, 2016).

On the other hand, regression analysis aims to estimate particular relationships between the target variables and the spectral response. It is used to predict the concentration of different constituents in a pixel, thus, enabling the visualisation of their spatial distribution in a specimen (Vigneau et al., 2011). Numerous regression models have been developed for analysing HSI data such as multiple linear regression (MLR; Delalieux et al., 2007), partial least squares regression (PLSR; Vigneau et al., 2011), binary logistic regression (BLR; Lu, Shimizu, Ishii, Washitani, & Omasa, 2012) and support vector regression (SVR; Malenovskỳ, Turnbull, Lucieer, & Robinson, 2015).

4. Recent applications

Recent applications of HSI, ranging from simple biochemical content estimation to monitoring of plant growth under controlled environment (Phenotyping) are presented in Table 1. The major applications were related to foliar content estimation, disease detection, variety identification, leaves monitoring, stress related studies, phenotyping and adoption of HSI in HTPPs. These applications are further discussed in the following subsections.

4.1. *Foliar biochemistry estimation*

Estimation of foliar biochemistry allows a better understanding of overall plant health. This is possible because of relationships between the biochemical processes such as photosynthesis, and the concentration of foliar biochemicals such as chlorophyll, water, nitrogen, lignin and cellulose (Curran, Dungan, & Peterson, 2001).

The reflectance information in the VIS and NIR regions makes the HSI an ideal modality for non-destructive foliar biochemistry estimation. To estimate the concentration of biochemicals, regression modelling such as PLSR is typically used. The regression method uses some selected spectra with known values for the foliar biochemicals to estimate model parameters. The obtained model parameters are then used to generate maps of the biochemical of interest to obtain its distribution at leaf and plant level.

Various applications on the estimation of biochemistry can be found in recent works. Most of the applications were related to the estimation of chlorophyll and nitrogen content. Nitrogen, being an integral part of amino acids is also a major component of chlorophyll. Since plants wither and die without amino acids, it is important to know the nitrogen and chlorophyll content in plants. There are different measurement techniques for measuring the nitrogen and chlorophyll content such as high-performance liquid chromatography (HPLC), fluorimetry, spectrometry etc. Point spectroscopy techniques are also used to perform the estimation. Most of the techniques used are tedious, destructive and invasive. On the other hand, HSI provides information in a rapid non-destructive sense which also allows time-series monitoring of changes in the concentration.

Min et al. (2008) designed a point spectroscopy system for estimating nitrogen content in plucked orange (*Citrus sinensis*) leaves. Wavelength ranges of 620–950 nm and 1400–2500 nm were chosen because of the presence of chlorophyll and protein spectral absorption bands. With a root mean square difference of 1.69 g kg^{-1} the system was successful in predicting the nitrogen content in the leaves. Furthermore, using a supervised approach, the authors were able to classify unknown leaf samples into low, medium and high nitrogen content with an accuracy of 70%.

For estimating the nitrogen content at the panicle initiation stage in rice plants *(in-vivo)*, Onoyama et al. (2013) used HSI in the spectral range of 400–1000 nm. They constructed a PLSR model based on the relationship between the reflectance combined with the cumulative temperature and nitrogen content. Later the model parameters were used to predict the nitrogen content. A $R^2 = 0.92$ and root mean squared error (RMSE) = 0.62 g m^{-2} was obtained from reflectance and temperature data gathered over a period of 2 years.

Similarly, Vigneau et al. (2011) estimated leaf nitrogen concentration from reflectance (400–1000 nm) spectra in wheat plants *(in-vivo)*. They first calibrated leaf nitrogen concentration and reflectance spectra of flat leaves grown in the greenhouse ($R^2 = 0.889$) and under field conditions ($R^2 = 0.881$). Later, they modelled the pooled dataset from greenhouse and field data to predict leaf nitrogen content ($R^2 = 0.875$). This model was used to generate spatial nitrogen maps to follow-up nitrogen dynamics at leaf level.

In an another work, Yu et al. (2014) used HSI (380–1030 nm) to extract distributions of total nitrogen content in pepper plants (plucked leaves). Using PLSR, the quantitative relationships between spectral data and the corresponding total

Table 1 – Recent applications of HSI for understanding functional plant traits. Some important applications of non-imaging hyperspectral reflectance measurements are also present.

Applications	Spectral range (nm)	Plant	Domain	Sensing modality	Plant trait/ Disease/Stress	Data analysis	Authors
Foliar biochemistry estimation	400–1000	*Ginkgo biloba*, *Zelkova serrata*	Laboratory (*Plucked leaves*)	Imaging	Chlorophyll and water	Correlation coefficients	Endo, Tamura, and Yasuoka (2001)
	620–950 and 1400–2500	Orange	Lab (*Plucked leaves*)	Non-imaging	Nitrogen	PLSR and Stepwise multiple linear regression	Min et al. (2008)
	400–1000	Wheat	Field and Greenhouse (*In-vivo*)	Imaging	Nitrogen	PLSR	Vigneau et al. (2011)
	450–850	Cucumber	Greenhouse (*Plucked leaves*)	Imaging	Chlorophyll	Vegetation indices	Xiaobo et al. (2011)
	400–1000	Rice	Field (*In-vivo*)	Imaging	Nitrogen	PLSR	Onoyama, Ryu, Suguri, and Iida (2013)
	380–1030	Pepper	Laboratory (*Plucked leaves*)	Imaging	Nitrogen	PLSR	Yu et al. (2014)
	380–1030	Oilseed rape	Laboratory (*Plucked leaves*)	Imaging	Soluble protein	PLSR	Zhang, Liu, Kong, and He (2015)
Leaf monitoring	400–1000	Spinach	Lab (*Plucked leaves*)	Imaging	Changes in pigments	PCA	Lara, Lleó, Diezma-Iglesias, Roger, and Ruiz-Altisent (2013)
	400–900	Corn	Lab (*Plucked leaves*)	Imaging	Monitored reflectance changes	Visual inspection	Lee, Huang, Yao, Thomson, and Bruce (2014)
Species identification	400–2400	Eucalyptus	Field (*In-vivo*)	Non-imaging	Discrimination	Derivatives, ratios and vegetation indices	Kumar et al. (2010)
	400–2500	*Prumus dulics*, *Annona squamosa*, *Psidum guajava*, *Ziziphus jujube*, *Mangifera indica* and *Butea monosperma*	Field (*In-vivo*)	Non-imaging	Classification	SVM	Varpe, Rajendra, Vibhute, Gaikwad, and Kale (2015)
Abiotic stress detection	380–930	Eucalyptus	Glasshouse and Field (*Plucked leaves*)	Imaging	Freezing	Linear regression	Nicotra, Hofmann, Siebke, and Ball (2003)
	430–890	Maize	Greenhouse and Field (*In-vivo*)	Imaging	Drought	SVM	Behmann, Steinrücken, et al. (2014)
	421–780	Soybean	Controlled growth chambers (*Plucked leaves*)	Imaging	Drought	PLSR	Mo et al. (2015)
	350–2500	Palm	Field (*In-vivo*)	Imaging	Hydrocarbon Seepage	Visual inspection	Jamaludin, Matori, and Myint (2015)
	325–1075	*Bryum pseudotri- 609 quetrum*, *Ceratodon purpureus and Schistidium antarctici*	Field (*In-vivo*)	Imaging	Drought	SVR and Vegetation indices	Malenovskỳ et al. (2015)
	350–2500	Potato	Outdoor controlled conditions (*In-vivo*)	Imaging	Drought	Vegetation indices	Gerhards, Rock, Schlerf, and Udelhoven (2016)
	300–1100	Wheat	Field (*In-vivo*)	Non-imaging	Ozone	Correlation analysis	Chi et al. (2016)

(*continued on next page*)

Table 1 – (*continued*)

Applications	Spectral range (nm)	Plant	Domain	Sensing modality	Plant trait/ Disease/Stress	Data analysis	Authors
Biotic stress detection	350–2500	Rice	Lab and Field (*In-vivo*)	Non-imaging	*Helminthosporium oryzae Breda. de Hann*	Reflectance ratios	Liu, Huang, and Tao (2008)
	400–1050	Sugar beet	Greenhouse (*In-vivo*)	Non-imaging	*Cercospora beticola*	SVM	Rumpf et al. (2010)
	400–1000	Sugar beet	Greenhouse (*In-vivo*)	Non-imaging	*Cercospora beticola*	Vegetation Indices	Mahlein et al. (2010)
	400–1000	Sugar beet	Greenhouse (*Plucked leaves*)	Imaging	*Cercospora beticola*	SAM	Mahlein, Steiner, Hillnhütter, Dehne, and Oerke (2012)
	400–1000	Sugar beet	Greenhouse (*Plucked leaves*)	Imaging	*Cercospora beticola*	Vegetation indices	Mahlein et al. (2013)
	380–1030	Tomato	Greenhouse (*Plucked leaves*)	Imaging	*Botrytis cinerea*	GA-PLS	Kong et al. (2014)
	380–1023	Tomato	Greenhouse (*Plucked leaves*)	Imaging	*Alternaria solani*, *Phytophthora infestans*	Extreme Learning Machine (ELM)	Xie, Shao, Li, and He (2015)
	400–1000	Apple	Field (*In-vivo*)	Imaging	Marssonina Coronaria	Hierarchical clustering	Posadas, Lee, Hong, and Kim (2015)
	400–2500	Oilseed rape (*Brassica napus* L.)	Controlled conditions (*Plucked leaves*)	Imaging	Fungal species of *Alternaria*	ANN	Baranowski et al. (2015)
	400–1000	Tomato	Laboratory (*Plucked leaves*)	Imaging	*Pseudomonas cichorii*	PCA	Rajendran et al. (2016)
	400–1000	Strawberry	Greenhouse (*In-vivo*)	Imaging	Anthracnose	SAM, Stepwise Discriminant Analysis and Self-developed Correlation Measure	Yeh et al. (2016)
	380–1023	Tobacco	Laboratory (*Plucked leaves*)	Imaging	Tobacco mosaic virus	SVM, ANN, ELM, Least Squares SVM, PLS-DA, Linear Discriminant Analysis and Random Forest	Zhu et al. (2016)
	380–1023	Banana	Laboratory (*In-vivo*)	Imaging	*Mycosphaerella fijiensis*	Visual Inspection	Ochoa et al. (2016)
Phenotyping	400–1000	Barley	Greenhouse (*Plucked leaves*)	Imaging	Host–pathogen interactions	SiVM	Kuska et al. (2015)
	400–900	Sugar beet	Greenhouse (*Plucked leaves*)	Imaging	Disease Resistant breeding	SAM	Leucker, Mahlein, Steiner, and Oerke (2016)
	400–1000	Barley	Greenhouse (*Plucked leaves*)	Imaging	Resistance breeding	Probabilistic topic models	Wahabzada et al. (2016)
	550–1750	Maize	Greenhouse (*In-vivo*)	Imaging	Biochemical traits	PLSR	Ge, Bai, Stoerger, and Schnable (2016)
	400–900	Grapevine	Greenhouse (*Plucked leaves*)	Imaging	Biochemical traits	SAM	Oerke et al. (2016)
	970–2500	Sugar beet	Greenhouse (*Plucked leaves*)	Imaging	Resistance breeding	ANN	Arens et al. (2016)
	400–1000	Sugar beet	Greenhouse (*Plucked leaves*)	Imaging	Disease Resistance breeding	Clustering	Leucker et al. (2017)

nitrogen contents in leaf, stem, root and whole plant were obtained. The obtained model had a correlation coefficient of $R^2 = 0.876$ and RMSE = 0.426. Finally, maps of the total nitrogen content of pepper plants were generated by using the model parameters obtained from PLSR.

For estimation of the chlorophyll content, Endo et al. (2001) used a HSI sensor in the 400–1000 nm wavelength region to collect images of *Ginko biloba* and *Zalkova serrata* (plucked leaves). $R^2 = 0.85$ and $R^2 = 0.79$ between chlorophyll a and the first derivative of the spectral reflectance in the neighbourhood of the red edge were obtained for *G. biloba* and *Z. serrata* respectively. The RMS error of the estimated chlorophyll a concentration was 4.80 $\mu g\ cm^{-2}$ and 3.05 $\mu g\ cm^{-2}$ respectively. Estimation of relative water content, however, was less successful compared to the prediction of chlorophyll due to the limited spectral range used in the work.

Similarly, Xiaobo et al. (2011) enabled identification and characterisation of relative chlorophyll content in cucumber leaves (plucked leaves) by using HSI in the range of 450–850 nm. The obtained maps showed a relatively low amount of chlorophyll at the leaf edges and higher amounts in the regions along the veins and areas of dark green tissues.

Zhang et al. (2015) used HSI (380–1030 nm) for rapid and non-destructive estimation of the soluble protein content of oilseed rape leaves (plucked leaves). A PLSR model, developed from the reflectance spectra and protein estimates provided a correlation coefficient of $R^2 = 0.9441$ with a RMSE of 0.1658 mg g^{-1}. HSI provided a clear map of soluble protein content within the rape leaves.

All these results prove that HSI is a valuable tool for non-destructive *in situ* foliar content prediction in living plants.

4.2. *Leaf monitoring*

The monitoring of the leaf structural and functional dynamics is important for exploration of plant traits in various disciplines of ecology, plant biology and plant growth analysis (Fiorani et al., 2012). Typically, traditional methods used for monitoring the leaves are based on the use of ecological sampling methods such as the quadrat technique. This sampling technique enables to obtain comparable samples from similar representative areas. The quadrat technique is time and labour demanding and prone to human errors. On the contrary, HSI can perform non-destructive real-time monitoring of leaves in larger areas and form an important step towards the development of automated leaf monitoring systems.

A study for exploring the potential of HSI for spinach leaf (plucked leaves) monitoring was performed by Lara et al. (2013). They used HSI (400–1000 nm) to monitor the ageing of spinach leaves through packaging films. They experimented with fifteen different spinach leaves inside Petri dishes covered with plastic films and stored them at 4 °C. HSI was acquired seven times during 21 days. Their results showed that HSI successfully could monitor the ageing effect of spinach leaves.

In a similar work, Lee et al. (2014) used HSI (400–900 nm) to monitor the leaf reflectance (plucked leaves) of excised corn leaves stored inside and outside a cooler. They performed the measurements after 15 min of excision, then again after 1, 2, 3, 4, 5, 6, and 24 h of excision. Each HS band was modelled independently using a piecewise function. Results showed that during the first hour, the storage did not have any influence on the spectral signature. However, after one hour the reflectance changed more for leaves stored inside the cooler than those outside, the cooler.

4.3. *Species identification*

Plant species identification is required for plants which are unidentified or unknown by the scientific world. The traditional approach used for species identification is the use of trained taxonomists, capable of examining specimens and provide taxonomic labels. However, the method is manually challenging because an expert on one species or its family may be unfamiliar with other species. Furthermore, the need exists for automated fast and non-destructive technologies to support species identification and to allow people with limited botanical training and expertise to perform this task (Cope, Corney, Clark, Remagnino, & Wilkin, 2012). The structural and biophysical characterisation of plants by HSI can play a significant role in identifying and distinguishing between different plant species.

Applications of HSI for species identification are still lacking but the potential of point spectroscopy for the task had already been proven. A work related to the use of point spectroscopy (400–2400 nm) for species identification was performed by Kumar et al. (2010), where discrimination between 11 eucalyptus species (*in-vivo*) was the goal. They recorded the reflectance signatures from 11 eucalyptus species in laboratory and identified significant differences between species in distinct wavelengths ranges. The major differences were identified regarding absolute reflectance, depths of absorption features and changes in the function of wavelength. The differences were more easily noticeable in first derivative spectra than in the reflectance spectra. The authors investigated the possibility of utilising vegetation indices used in remote sensing for discriminating between species. Similarly, Varpe et al. (2015) used point spectroscopy (400–2500 nm) to develop a plant species identification system (*in-vivo*). They were able to successfully identify various plant species (*Prumus dulics*, *Annona squamosa*, *Psidum guajava*, *Ziziphus jujube*, *Mangifera indica*, *Butea monosperma*) with an accuracy of 91%.

4.4. *Stress detection*

Plant stress is induced by the negative influence of various external factors and effects plant growth, productivity, reproductive capacity or survival. There are numerous factors causing plant stress, and these can be categorised into two classes, i.e. biotic and abiotic factors. Abiotic or environmental stress factors are physical or chemical in nature, e.g. light, temperature etc., whereas biotic stress factors are biological, e.g. insects or spread of fungal diseases.

Whether biotic or abiotic, identification of plant stress and its treatment is of crucial importance for crop development. Typically, the symptoms resulting from stress are initially not visible to human eyes, and only become apparent when plant health is already seriously affected. Therefore, there exists a need for non-destructive technologies that can provide an

early detection of symptoms resulting from stress. HSI being a non-destructive technology has recently emerged as the potential tool for early detection of symptoms resulting from abiotic (Römer et al., 2012) and biotic (Mahlein et al., 2013) stresses. Any stress changes the photosynthetic activity of the plants which results in changes in concentrations of pigments or biochemical constituents, changes which can be observed in the reflectance spectra.

4.4.1. *Abiotic stress detection*

Nicotra et al. (2003) studied the relation between spatial patterns of freezing and concentrations of chlorophyll in Eucalyptus (plucked leaves). Spatial patterns of pigments were determined by conventional extraction techniques along with HSI (380–930 nm). Obtained spatial maps of frost-affected leaves showed that the chlorophyll content was highest near the leaf centres and decreased toward the leaf tips. The decrease in chlorophyll content was related with freezing-related tissue damage and interactions between light and temperature stress and was identified as shifts in chlorophyll a/b ratios and increases in red pigmentation due to the accumulation of anthocyanin.

In a work related to detection of stress induced by drought, Behmann, Steinrücken, et al. (2014) used HSI (430–890 nm) to explore the early symptoms of drought in barley plants (*in-vivo*). They used unsupervised learning to separate distinct spectral features related to different stages of stress response and progressive senescence. Based on changes related to the degradation of pigments, it was possible to detect drought stress in the plants.

Mo et al. (2015) used fluorescence HSI (421–780 nm) and a PLSR model for detecting drought stress in soybean (plucked leaves). The features obtained from the model were used to generate spatial maps of soybean cultivars for the period of the drought treatment. Analysis of the spatial maps provided a clear discrimination of drought stress in the soybean cultivars with accuracies of 0.973% and 0.969 %for an 8-day and 6-day treatment group respectively.

Malenovskỳ et al. (2015) used HSI (325–1075 nm) for the spatial assessment of moss-bed health (*in-vivo*). Reflectance of three dominant Antarctic mosses *Bryum pseudotriquetrum*, *Ceratodon purpureus* and *Schistidium antarctici* were measured during a drought stress period. Turf chlorophyll a and b, water content and leaf density were selected as quantitative stress indicators. The processing of HSI field measurements provided small-scale maps of relative moss vigour. Furthermore, the authors concluded that HSI could be used for long-term monitoring of Antarctic moss-bed health.

With a multi-sensor approach, Gerhards et al. (2016) used HS (350–2500 nm) thermal cameras and a VNIR/SWIR spectrometer for detecting drought stress in potato plants (*in-vivo*). 30 plants were watered normally, and another 30 were stressed with drought. Various vegetation indices were computed, and the best was selected for discriminating plants under drought. Results showed that the fastest detection was obtained with the use of indices based on temperature and NIR/SWIR wavelengths mainly related to water content. The study concluded that drought stress detection is feasible with the use of indices explaining leaf temperature, water content and spectral emissivity.

To detect stress resulting from seepage of hydrocarbon in palm tree (*in-vivo*), Jamaludin et al. (2015) used point spectroscopy (350–2500 nm). A total of 50 trees were used for the study of which 40 trees were stimulated with hydrocarbon microseepage, and the remaining ten trees were left as the control. Spectral data were acquired on the first, 60th and 90th day of the plantation. The reflectance spectra along with the 1-st derivatives were analysed in the red-edge and visible regions, to determine the effects of hydrocarbon microseepage. Results indicated that trees with ten % hydrocarbon microseepage encountered mild stress, while more than 40% hydrocarbon was lethal for the trees.

Chi et al. (2016) used point spectroscopy (300–1100 nm) data to detect ozone (O_3) induced stress. Four wheat cultivars were studied in open-air fields with different O_3 concentrations (*in-vivo*). Results showed that the O_3 stress caused a significant decrease in leaf thickness and pigment concentrations. Moreover, the effects of O_3 stress on physiological variables and reflectance characteristics were found to be wheat cultivar-specific.

4.4.2. *Biotic stress detection*

The need for automatic, non-destructive and rapid methods for early detection of biotic stresses such as plant diseases is important for plant protection. An early detection of a disease can help in preventing its spread and can help in effective reduction of qualitative and quantitative losses (Mahlein, 2016). Being a relatively new technology for exploring plants traits, HSI is gaining interest for its application in plant pathology (Bock et al., 2010). Typically, the diseases in plants are quantified regarding intensity, prevalence, incidence and severity. The ability of HSI to capture the changes in leaf spectral reflectance caused by plant diseases can help in better understanding of the plant symptoms under particular diseases. Also, HSI can be used for reliable, precise and accurate estimation of disease severity, assessment of crop germplasm for disease resistance, yield loss prediction, monitoring and forecasting of epidemics, and to understand fundamental biological processes (Bock et al., 2010).

To estimate and characterise the severity of fungal brown spot disease in rice, Liu et al. (2008) used point spectroscopy (350–2500 nm) of rice in the laboratory and the field (*in-vivo*). Later, various spectral regions sensitive to rice brown spot, infected by *Bipolaris oryzae* (*Helminthosporium oryzae Breda. de Hann*) were characterised. Three reflectance ratios R702/R718, R692/R530, R692/R732 were found to be best for estimating the disease severity of rice brown spot at the leaf and canopy levels.

Similarly, Rumpf et al. (2010) used point spectroscopy (400–1050 nm) for early detection of three sugar beet diseases (cercospora leaf spot (CLS), leaf rust and powdery mildew). They used the HSI for recording images from healthy and inoculated leaves with the corresponding pathogens, respectively for 21 days. As features to the automatic classification methodology based on SVM, nine different spectral vegetation indices were used. A clear early differentiation between healthy and inoculated plants as well as among the different diseases was obtained with a classification accuracy of 97%. The potential of point spectroscopy (400–1000 nm) for the same three sugar beet diseases (*in-vivo*) was examined by

Mahlein et al. (2010). In their later work, Mahlein et al. (2012) used HSI (400–1000 nm) to relate leaf characteristics and spectral reflectance of sugar beet leaves diseased with CLS, powdery mildew and leaf rust at different development stages (plucked leaves). They concluded that the influence of pathogens on leaf reflectance could be related to the developmental stage of the diseases. Furthermore, with SAM classification, a clear differentiation between distinct ontogenetic stages was obtained. As a follow-up, Mahlein et al. (2013) developed spectral indices for the detection of diseases in sugar beet plants (plucked leaves) (400–1000 nm).

Kong et al. (2014) examined the possibility of HSI (380–1030 nm) for detection of peroxidase (POD) activity in tomato leaves (plucked leaves) which were infected with *Botrytis cinerea*. POD is an important indicator of disease stress. Genetic algorithm partial least square (GA-PLS) was applied to select the optimal wavelengths. Later, an ELM model was used at the selected wavelengths and provided R^2 and RMSE of 0.86 and 466 respectively. Similarly, Xie et al. (2015) used HSI (380–1023 nm) to image one hundred and twenty healthy, one hundred and twenty early blight and seventy late blight diseased tomato leaves (plucked leaves), and obtained a classification accuracy of 71.8%. Rajendran et al. (2016) used HSI (400–1000 nm) for investigating different levels of severity of *Pseudomonas cichorii* infection in tomato plants (plucked leaves). In their experiments, the plants were inoculated with different cell densities of *P. cichorii*. Later, VNIR and chlorophyll fluorescence HSI were acquired. They concluded that the *P. cichorii* infection severity can be detected by before the onset of visible symptoms.

Besides rice, sugar beet and tomato plants, other species were subject of research on the spectral analysis of disease stresses. Baranowski et al. (2015) used a multi-sensor approach to understanding the underlying symptoms of stress caused by fungal species in oilseed rape (plucked leaves). They used thermal (8000–13,000 nm), VNIR and SWIR HSI for recording the spectral characteristics of inoculated leaves and non-treated plants. They found that the spectral characteristics in the SWIR range (1000–2500 nm) significantly differed for the leaves inoculated with *Alternaria dauci* compared to the other species of *Alternaria* as well as leaves of non-treated plants. Furthermore, a classification accuracy of 95% was obtained using second-derivative spectral information along with back-propagation neural networks. Posadas et al. (2015) used HSI (400–1000 nm) for detecting apple marssonina blotch (AMB) disease (*in-vivo*). They acquired spectral data in the NIR range since it can capture information on various plant biochemicals that affect health, such as moisture, nitrogen, and other nutrients. The data were used for calibrating a model for early detection of AMB, and NIR-HSI was shown to be a promising tool for early detection of various plant diseases. In Yeh et al. (2016), different infection stages of anthracnose were studied in strawberries (*in-vivo*). Three different infection stages (healthy, incubation and symptomatic stages) were investigated using HSI (400–1000 nm), and a classification accuracy of 80% was obtained. Furthermore, the study identified significant wavelengths (551, 706, 750 and 914 nm) which can be used to develop a cheaper multispectral system with similar classification performance. Zhu et al. (2016) used HSI (380–1023 nm) for early detection and classification of the tobacco mosaic virus (TMV) disease using different machine-learning algorithms. Images from healthy leaves and leaves inoculated with TMV were acquired for seven days (plucked leaves). Results provided a clear distinction between healthy and diseased tobacco leaves with a classification accuracy of 95%. Finally, Ochoa et al. (2016) successfully used HSI (380–1023 nm) for *in-vivo* detection of *Black Sigatoka* pre-symptomatic responses in banana leaves (*in-vivo*).

4.5. *Phenotyping*

Plant phenotyping is the act of monitoring of the genetic characteristics of a plant when interacting with its environment. Typically, this interaction influences plant structural and functional traits that determine the plant performance regarding biomass and yield Dhondt, Wuyts, and Inzé (2016). Traditional methods for phenotyping are still time-consuming, labour intensive and destructive, and there is a need for fast and non-destructive high throughput technologies. HSI, being capable of extracting spectral and spatial information is an emerging potential tool for studying plant traits. Spanning a broad range of the EMR in a non-destructive way, HSI has the potential to capture both structural and functional traits to support the need of phenotyping.

In a recent work, Kuska et al. (2015) used a data-driven phenotyping approach based on HSI to evaluate host–pathogen interactions and discrimination of barley (plucked leaves) genotypes differing in susceptibility to powdery mildew. They used a HS (400–1000 nm) microscope to determine the spectral changes on the leaf at the cellular level of barley during resistance reactions against powdery mildew. Leucker et al. (2016) used HSI (plucked leaves) for improvement of lesion phenotyping in *Cercospora beticola*-sugar beet interactions. Subregions corresponding to lesions were identified in the spectral region of 400–900 nm. In an additional work, Leucker et al. (2017) used a HS (400–1000 nm) microscopy for characterising the temporal and spatial development of CLS lesions in two genotypes of sugar beet (plucked leaves). Fast and abrupt changes in spectral reflectance resulted from the development of lesions. Clustering of HS signatures was performed for automatically revealing resistance characteristics. Results proved the potential of HSI to differentiate CLS dynamics and lesion composition and opened doors for improved resistance breeding by objective and precise plant phenotyping. All these results showed that HSI is a potential tool to improve the screening process during resistance breeding.

Wahabzada et al. (2016) used HSI (400–1000 nm) for phenotyping and monitoring barley plant responses to three foliar diseases *Pyrenophora teres*, *Puccinia hordei*, and *Blumeria graminis hordei* (plucked leaves). They converted the HS characteristics of diseased plants into the corpus of text documents for probabilistic topic modelling. Based on regularised topic models, it was possible to automatically track the development of the three foliar diseases of barley. In a multi-sensor approach, Ge et al. (2016) used automated high throughput RGB and HSI (550–1750 nm) for characterising temporal dynamics of plant growth, water use, and leaf water content of two maize genotypes under two different water treatments

(*in-vivo*). They used RGB images to estimate projected plant area, which was further correlated ($R^2 > 0.95$) with destructively measured plant shoot fresh weight, dry weight and leaf area. HSI of plants were correlated with leaf water content. Obtained model parameters were used successfully to predict the leaf water content for both genotypes ($R^2 = 0.81$ and 0.92). In an application of grapevine breeding, Oerke et al. (2016) used HSI (plucked leaves) (400–900 nm) under controlled conditions for characterising the response of cultivars *Mueller-Thurgau*, *Regent and Solaris* to P. viticola. The spatial maps provided by the HSI contained enhanced relevant information for disease detection compared to a non-imaging modality. The different spectral indices provided information related to the chlorophyll content, photosynthetic activity and relative water content of leaf tissues. Arens et al. (2016) used HSI (plucked leaves) (970–2500 nm) in combination with metabolite profiles to analyse sugar beet genotypes. The HSI provided a clear detection of *C. beticola* with accuracies of 98.5–99.9% and metabolite analysis successfully revealed defence response regarding alteration of metabolites by the host.

All these results show that HSI is a potential tool to improve the screening process during resistance breeding and to accomplish a speed up of the selection of resistant cultivars against specific diseases.

4.6. *High-throughput phenotyping platforms*

The availability of complex non-destructive sensors and technical advancement in management, storage and integration of multisource data has enabled the synergistic monitoring of plants growth dynamics (Cozzolino & Roberts, 2016). Incorporating different sensors and variable control environments, various HTPPs are being developed by international companies and public plant research institutions throughout the globe (Araus & Cairns, 2014). For more specific information regarding the HTPPs, readers are encouraged to access web pages available from some recently developed platforms:

(i) PHENOVISION from Vlaams Instituut voor Biotechnologie (VIB), Belgium (PHENOVISION)
(ii) PlantScan from Commonwealth Scientific and Industrial Research Organisation (CSIRO), Australia (CSIRO)
(iii) PlantScreen from Photon System Instruments (PSI), Czech Republic (PlantScreen)
(iv) Field phenotyping platform, ETH Zurich, Switzerland (Field)
(v) Lemnatec's plant phenotyping platform at National Plant Phenomics Centre, Aberystwyth University, United Kingdom (Lemnatec)
(vi) The Bellwether Foundation Phenotyping Facility, Rothamsted, Research Center Julich, Germany (Bellwether)

HTPPs typically include automated greenhouse facilities like growth chambers with robotics, precise environmental control and a combination of sensors to explore plant growth and performance (Araus & Cairns, 2014).

To quantify genotypes, the HTPPs provide time-series measurements, monitoring growth parameters, increased yield and adaptability to abiotic or biotic stresses on individual plants of a particular phenotype interacting with its surrounding environment (Fahlgren, Gehan, & Baxter, 2015; Sytar et al., 2017). Non-destructive sensors and advances in data processing have revolutionised the development of HTPPs that became major tools in plant phenotyping studies. However, to efficiently utilise multi-sensor systems in HTPPs, well-planned experimentation is required to obtain phenomics data which can be linked with the results of metabolomic, molecular or physiological parameters (Walter, Liebisch, & Hund, 2015). HSI is a unique multi-purpose sensor with applications on foliar content estimation, disease detection, variety identification, growth monitoring, heavy metal detection and stress related studies. Many of the applications of HSI are adapted from the remote sensing domain. Methodologies and conclusions already existing in remote sensing can be adopted and adjusted for close range applications (Walter et al., 2015). HSI can become an integral part of HTPPs for exploring the genetic variabilities in plants efficiently and reliably (Sytar et al., 2017).

5. Technical challenges

In the last decade, HSI is increasingly being applied for assessment of functional plant traits in close range settings. Nevertheless, as an emerging application, it faces some major challenges limiting its full potential. Many of the limitations are either related to the technical complexity of the imaging setup or the nature of the samples to be imaged.

To date, the most common imaging setup used for close range HSI acquisition is based on a push-broom movement of the sensor. In this technique, the acquisition of HSI is slower than other conventional RGB, thermal and NIR cameras. Another issue with the push-broom technique is the possibility of having signal disturbance due to the relative movement between the sample and the imaging platform. One of the common, resulting effects associated with this problem is line stripping. Usually, these effects can be handled by dark and white reference calibration, but if the effect is too prominent, a proper de-noising technique (Rogass et al., 2014) is needed to recover the damaged image information. Furthermore, as the amount of data generated by HSI is enormous, managing experimental data is a challenging task, and it requires additional costs in handling the storage and transmission. Therefore, efficient compression should be applied to these data to ensure ease of access and transportation of the generated data (Tang & Pearlman, 2006).

HSI being used in exploring plants traits such as water content, nutrient status, disease infections and insect damages, has a high cost compared to other sensors such as RGB cameras, point spectrophotometers etc (Lee, 2015). A common approach is to use HSI in an exploratory first phase to identify relevant application-specific wavelengths, and then further on use, this information to design and apply cheaper multispectral systems (Mahlein et al., 2013; Mutka & Bart, 2015).

When applied particularly in close range laboratory settings, HSI suffers from disturbances caused by the applied illumination, and therefore, sensor calibration concerning the illumination is a major concern. Dark and white reference

calibration is frequently required which consequently slows down the acquisition process. A specific close range challenge is that the reflectance strongly depends on the distance and the orientation of each ROI towards the light source and camera. Further complications are due to complex leaf curvatures, local surface irregularities and the complex 3D geometry of plants causing multiple reflections and self-shading, which influence the underlying signal from any biochemical parameter or biophysical process. The complex geometry and its interaction with the light for artificial and natural illumination can be understood with Fig. 6. It can be seen in Fig. 6(a.) that in artificial illumination conditions, the top of a plant receives more illumination than the bottom. These differences in illumination cause additive and multiplicative effects in the reflectance spectrum generated by the plants (Mohd Shahrimie et al., 2016). In field conditions, this distance effect is not apparent, since the light source is very far away, but the imaging is largely affected by the location of the sun, i.e. the angle of the sun rays towards the nadir.

To deal with these illumination effects, various technical solutions are being introduced by different researchers. Behmann, Mahlein, et al. (2014) proposed a combination of HSI with 3D point clouds obtained from a laser triangulation scanner as a promising approach to deal with this problem. These 3D plant models were used by Roscher et al. (2016) for the detection of *Cercospora* leaf spot disease symptoms on sugar beet plants. An improvement in detection of disease symptoms was obtained by incorporating the local inclination information from the 3D plant models. However, the spatial resolution that can be obtained with 3D cloud points is much lower than the HSI data. Also, since the HSI and the geometric information are not acquired simultaneously, even the smallest motion artefact or misregistration lead to significant inaccuracies.

When no additional sensor to support the generation of a 3D model is available, other correction methods are required. In outdoor environments, Vigneau et al. (2011) used normalisation (SNV) to remove leaf inclination effects, considerably improving the estimation of nitrogen content in wheat plants. Similarly, Mohd Shahrimie et al. (2016) modelled distance and orientation effects in laboratory environments by the inverse square law and Lambert's cosine law and used the SNV to correct for these effects. In a different approach, Jay, Bendoula, Hadoux, Féret, and Gorretta (2016) incorporated two additional parameters, incident angle and illumination zenith angle in the directional hemispherical reflectance model of leaf optical properties (PROSPECT) to deal with the bidirectional reflectance effects in close-range HSI. They validated this model using VNIR and SWIR HSI of various leaf species and obtained accurate maps of chlorophyll content, water thickness, leaf mass per unit area and leaf orientation.

6. Conclusion

The ability of HSI to provide integrated spatial and spectral information offers a perfect combination of rapid non-destructive assessment of plant traits. In the VIS region of the electromagnetic spectrum, the spectral information is majorly dominated by pigments while in the NIR, the information is related to different biochemical constituents such as water, starch, protein etc. A wide range of emerging applications of HSI, on whole plants or on plucked leaves, such as foliar content estimation, disease detection, species identification, growth monitoring, stress related studies, phenotyping and adoption of HSI in HTPPs, prove that HSI is a potential tool for rapid and non-destructive exploration of plant traits.

Apart from being a costly technique, HSI is still in its initial stage of development for close range application to plants and faces some technical difficulties. These include illumination effects resulting from the complex geometry of plants, overlaying the underlying biophysical and biochemical information in the spectra. Various methods such as 3D plant models, spectral normalisation and physically based models are being

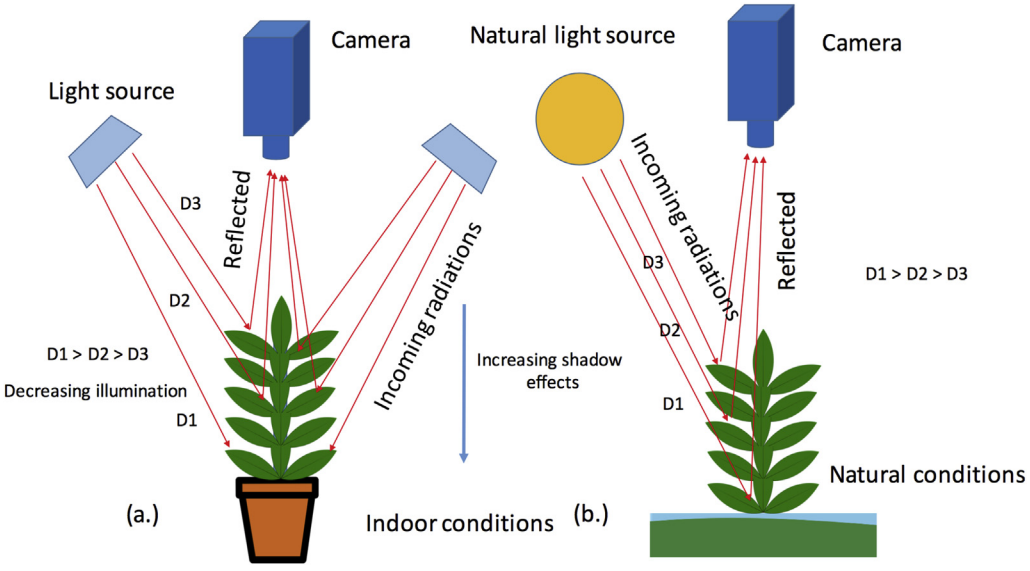

Fig. 6 – An illustration explaining the interaction of light with the complex plant geometry for (a.) artificial illumination conditions and (b.) natural agriculture conditions.

developed to deal with these effects. However, there is still no standard method to deal with these illumination effects. Another technical difficulty is related to the storage of the vast amount of data generated from the imaging. Therefore, efficient HSI data compression methods are needed to keep the experimental data record.

The use of HSI in close range for exploring plant traits benefits from earlier successes of HSI in remote sensing and from the state-of-the-art in point spectroscopy, from which many existing processing techniques can be adapted to close-range HSI. To prove the potential of HSI, more applications and new techniques which are accurate for close range HSI are needed. Opportunities also exist for developing standard procedures to remove the illumination effects from the images and for performing compression of HSI. With the advancement in sensor technology and data analysis, it can be expected that HSI will become a primary tool for exploring functional plant traits.

Acknowledgement

Puneet Mishra acknowledges the financial support from INDIA4EU2 project of Erasmus Mundus during his stay at Technical University of Madrid, Spain (http://www.india4eu.eu/). Mohd Shahrimie M. A. acknowledges the support of the Academic Staff Training Scheme (ASTS) of the Universiti Sains Malaysia and the Ministry of Higher Education of Malaysia.

REFERENCES

Amigo, J. M., Babamoradi, H., & Elcoroaristizabal, S. (2015). Hyperspectral image analysis. A tutorial. *Analytica Chimica Acta, 896*, 34–51.

Amigo, J. M., Marti, I., & Gowen, A. (2013). Hyperspectral imaging and chemometrics: A perfect combination for the analysis of food structure, composition and quality. In *Data handling in science and technology* (Vol.28, pp. 343–370).

Apelt, F., Breuer, D., Nikoloski, Z., Stitt, M., & Kragler, F. (2015). Phytotyping4d: A light-field imaging system for non-invasive and accurate monitoring of spatio-temporal plant growth. *The Plant Journal, 82*, 693–706.

Araus, J. L., & Cairns, J. E. (2014). Field high-throughput phenotyping: The new crop breeding frontier. *Trends in Plant Science, 19*, 52–61.

Arens, N., Backhaus, A., Döll, S., Fischer, S., Seiffert, U., & Mock, H.-P. (2016). Non-invasive presymptomatic detection of Cercospora beticola infection and identification of early metabolic responses in sugar beet. *Frontiers in Plant Science, 7*.

Bannon, D., & Thomas, R. (2005). Harsh environments dictate design of imaging spectrometer. *Laser Focus World, 41*, 93–97.

Baranowski, P., Jedryczka, M., Mazurek, W., Babula-Skowronska, D., Siedliska, A., & Kaczmarek, J. (2015). Hyperspectral and thermal imaging of oilseed rape (brassica napus) response to fungal species of the genus alternaria. *PLoS One, 10*, 1–19.

Barnes, R., Dhanoa, M., & Lister, S. J. (1989). Standard normal variate transformation and de-trending of near-infrared diffuse reflectance spectra. *Applied Spectroscopy, 43*, 772–777.

Behmann, J., Mahlein, A.-K., Paulus, S., Kuhlmann, H., Oerke, E.-C., & Plümer, L. (2014). Generation and application of hyperspectral 3d plant models. In *European conference on computer vision* (pp. 117–130). Springer.

Behmann, J., Mahlein, A.-K., Rumpf, T., Römer, C., & Plümer, L. (2015). A review of advanced machine learning methods for the detection of biotic stress in precision crop protection. *Precision Agriculture, 16*, 239–260.

Behmann, J., Steinrücken, J., & Plümer, L. (2014). Detection of early plant stress responses in hyperspectral images. *ISPRS Journal of Photogrammetry and Remote Sensing, 93*, 98–111.

Bellwether. https://www.danforthcenter.org/scientists-research/core-technologies/phenotyping. (Last accessed 7 October 2017).

Bergsträsser, S., Fanourakis, D., Schmittgen, S., Cendrero-Mateo, M. P., Jansen, M., Scharr, H., et al. (2015). Hyperart: Non-invasive quantification of leaf traits using hyperspectral absorption-reflectance-transmittance imaging. *Plant Methods, 11*, 1.

Blackburn, G. A. (2007). Hyperspectral remote sensing of plant pigments. *Journal of Experimental Botany, 58*, 855–867.

Bock, C., Parker, P., Cook, A., & Gottwald, T. (2008). Visual rating and the use of image analysis for assessing different symptoms of citrus canker on grapefruit leaves. *Plant Disease, 92*, 530–541.

Bock, C., Poole, G., Parker, P., & Gottwald, T. (2010). Plant disease severity estimated visually, by digital photography and image analysis, and by hyperspectral imaging. *Critical Reviews in Plant Sciences, 29*, 59–107.

Bucksch, A., Burridge, J., York, L. M., Das, A., Nord, E., Weitz, J. S., et al. (2014). Image-based high-throughput field phenotyping of crop roots. *Plant Physiology, 166*, 470–486.

Burger, J. (2006). *Hyperspectral NIR image analysis volume 2006*.

Burger, J. (2009). Replacement of hyperspectral image bad pixels. *NIR News, 20*, 19–21.

Busemeyer, L., Mentrup, D., Möller, K., Wunder, E., Alheit, K., Hahn, V., et al. (2013). Breedvisiona multi-sensor platform for non-destructive field-based phenotyping in plant breeding. *Sensors, 13*, 2830–2847.

Chen, Z.-P., Morris, J., & Martin, E. (2006). Extracting chemical information from spectral data with multiplicative light scattering effects by optical path-length estimation and correction. *Analytical Chemistry, 78*, 7674–7681. PMID: 17105158.

Chi, G., Huang, B., Shi, Y., Chen, X., Li, Q., & Zhu, J. (2016). Detecting ozone effects in four wheat cultivars using hyperspectral measurements under fully open-air field conditions. *Remote Sensing of Environment, 184*, 329–336.

Cope, J. S., Corney, D., Clark, J. Y., Remagnino, P., & Wilkin, P. (2012). Plant species identification using digital morphometrics: A review. *Expert Systems with Applications, 39*, 7562–7573.

Cozzolino, D., & Roberts, J. (2016). Applications and developments on the use of vibrational spectroscopy imaging for the analysis, monitoring and characterisation of crops and plants. *Molecules, 21*, 755.

CSIRO. http://www.plantphenomics.org.au/services-/plantscan. (Last accessed 7 October 2017).

Curran, P. J., Dungan, J. L., & Peterson, D. L. (2001). Estimating the foliar biochemical concentration of leaves with reflectance spectrometry: Testing the kokaly and clark methodologies. *Remote Sensing of Environment, 76*, 349–359.

Delalieux, S., van Aardt, J. A., Zarco-Tejada, P. J., Kempeneers, P., Verstraeten, W. W., & Coppin, P. (2007). Development of robust hyperspectral indices for the detection of deviations of normal plant state. In *EARSeL eProceedings* (vol. 6, p. 82).

Dhondt, S., Gonzalez, N., Blomme, J., De Milde, L., Van Daele, T., Van Akoleyen, D., et al. (2014). High-resolution time-resolved imaging of in vitro arabidopsis rosette growth. *The Plant Journal, 80*, 172–184.

Dhondt, S., Wuyts, N., & Inzé, D. (2016). Cell to whole-plant phenotyping: The best is yet to come. *Trends in Plant Science, 18*, 428–439.

Edelman, G., Gaston, E., Van Leeuwen, T., Cullen, P., & Aalders, M. (2012). Hyperspectral imaging for non-contact analysis of forensic traces. *Forensic Science International, 223*, 28–39.
ElMasry, G., Wang, N., & Vigneault, C. (2009). Detecting chilling injury in red delicious apple using hyperspectral imaging and neural networks. *Postharvest Biology and Technology, 52*, 1–8.
Endo, T., Tamura, M., & Yasuoka, Y. (2001). Spatial estimation of biochemical parameters of leaves with hyperspectral imager. In *Paper presented at the 22nd Asian conference on remote sensing* (Vol. 5, p. 9).
Fahlgren, N., Gehan, M. A., & Baxter, I. (2015). Lights, camera, action: High-throughput plant phenotyping is ready for a close-up. *Current Opinion in Plant Biology, 24*, 93–99.
Field. http://www.kp.ethz.ch/infrastructure/fip.html. (Last accessed 7 October 2017).
Feret, J.-B., François, C., Asner, G. P., Gitelson, A. A., Martin, R. E., Bidel, L. P., et al. (2008). Prospect-4 and 5: Advances in the leaf optical properties model separating photosynthetic pigments. *Remote Sensing of Environment, 112*, 3030–3043.
Fiorani, F., Rascher, U., Jahnke, S., & Schurr, U. (2012). Imaging plants dynamics in heterogenic environments. *Current Opinion in Biotechnology, 23*, 227–235.
Furbank, R. T., & Tester, M. (2011). Phenomics technologies to relieve the phenotyping bottleneck. *Trends in Plant Science, 16*, 635–644.
Ge, Y., Bai, G., Stoerger, V., & Schnable, J. C. (2016). Temporal dynamics of maize plant growth, water use, and leaf water content using automated high throughput rgb and hyperspectral imaging. *Computers and Electronics in Agriculture, 127*, 625–632.
Geladi, P., Burger, J., & Lestander, T. (2004). Hyperspectral imaging: Calibration problems and solutions. *Chemometrics and Intelligent Laboratory Systems, 72*, 209–217.
Gendrin, C., Roggo, Y., & Collet, C. (2008). Pharmaceutical applications of vibrational chemical imaging and chemometrics: A review. *Journal of Pharmaceutical and Biomedical Analysis, 48*, 533–553.
Gerhards, M., Rock, G., Schlerf, M., & Udelhoven, T. (2016). Water stress detection in potato plants using leaf temperature, emissivity, and reflectance. *International Journal of Applied Earth Observation and Geoinformation, 53*, 27–39.
Gonzalez, R. C., Woods, R., & Eddins, S. (2009). *Digital image processing using matlab* (Vol. 2).
Gowen, A. A., Feng, Y., Gaston, E., & Valdramidis, V. (2015). Recent applications of hyperspectral imaging in microbiology. *Talanta, 137*, 43–54.
Gowen, A., O'Donnell, C., Cullen, P., Downey, G., & Frias, J. (2007). Hyperspectral imaging an emerging process analytical tool for food quality and safety control. *Trends in Food Science and Technology, 18*, 590–598.
Guiñón, J. L., Ortega, E., García-Antón, J., & Pérez-Herranz, V. (2007). Moving average and savitzki-golay smoothing filters using mathcad. In *Papers ICEE, 2007*.
Hadoux, X., Gorretta, N., & Rabatel, G. (2012). Weeds-wheat discrimination using hyperspectral imagery. In *CIGR-ageng 2012, international conference on agricultural engineering* (pp. 6–p).
Hernández-Sánchez, N., Moreda, G. P., Herre-ro Langreo, A., & Melado-Herreros, Á. (2016). Assessment of internal and external quality of fruits and vegetables. In N. Sozer (Ed.), *Imaging technologies and data processing for food engineers* (pp. 269–309). Cham: Springer International Publishing.
Hillnhütter, C., Mahlein, A.-K., Sikora, R. A., & Oerke, E.-C. (2012). Use of imaging spectroscopy to discriminate symptoms caused by Heterodera schachtii and Rhizoctonia solani on sugar beet. *Precision Agriculture, 13*, 17–32.
Hughes, G. P. (1968). On the mean accuracy of statistical pattern recognizers. *Information Theory, IEEE Transactions on, 14*, 55–63.
Jacquemoud, S., & Baret, F. (1990). Prospect: A model of leaf optical properties spectra. *Remote Sensing of Environment, 34*, 75–91.
Jacquemoud, S., & Ustin, S. L. (2001). Leaf optical properties: A state of the art. In *8th international symposium of physical measurements & signatures in remote sensing* (pp. 223–332).
Jamaludin, M. I., Matori, A. N., & Myint, K. C. (2015). Application of nir to determine effects of hydrocarbon microseepage in oil palm vegetation stress. In *2015 international conference on space science and communication (IconSpace)* (pp. 215–220). IEEE.
Jay, S., Bendoula, R., Hadoux, X., Féret, J.-B., & Gorretta, N. (2016). A physically-based model for retrieving foliar biochemistry and leaf orientation using close-range imaging spectroscopy. *Remote Sensing of Environment, 177*, 220–236.
Jay, S., Hadoux, X., Gorretta, N., & Rabatel, G. (2014). Potential of hyperspectral imagery for nitrogen content retrieval in sugar beet leaves. In *, Vol. 2014. AgEng* (p. 8).
Jensen, J. (2007). *Remote sensing of the environment: An earth resource perspective*. Upper Saddle River, NJ: Pearson Prentice Hall.
de Juan, A., Maeder, M., Hancewicz, T., Duponchel, L., & Tauler, R. (2009). Chemometric tools for image analysis. In *Infrared and Raman spectroscopic imaging*. Wiley-VCH Verlag GmbH and Co. KGaA.
Kokaly, R. F., & Clark, R. N. (1999). Spectroscopic determination of leaf biochemistry using band-depth analysis of absorption features and stepwise multiple linear regression. *Remote Sensing of Environment, 67*, 267–287.
Kong, W., Liu, F., Zhang, C., Bao, Y., Yu, J., & He, Y. (2014). Fast detection of peroxidase (pod) activity in tomato leaves which infected with botrytis cinerea using hyperspectral imaging. *Spectrochimica Acta A: Molecular and Biomolecular Spectroscopy, 118*, 498–502.
Kumar, L., Skidmore, A. K., & Mutanga, O. (2010). Leaf level experiments to discriminate between eucalyptus species using high spectral resolution reflectance data: Use of derivatives, ratios and vegetation indices. *Geocarto International, 25*, 327–344.
Kuska, M., Wahabzada, M., Leucker, M., Dehne, H.-W., Kersting, K., Oerke, E.-C., et al. (2015). Hyperspectral phenotyping on the microscopic scale: Towards automated characterization of plant-pathogen interactions. *Plant Methods, 11*, 1.
Lara, M., Lleó, L., Diezma-Iglesias, B., Roger, J.-M., & Ruiz-Altisent, M. (2013). Monitoring spinach shelf-life with hyperspectral image through packaging films. *Journal of Food Engineering, 119*, 353–361.
Lee, W. S. (2015). Plant health detection and monitoring. In *Hyperspectral imaging technology in food and agriculture* (pp. 275–288). Springer.
Lee, M., Huang, Y., Yao, H., Thomson, S. J., & Bruce, L. M. (2014). Effects of sample storage on spectral reflectance changes in corn leaves excised from the field. *Journal of Agricultural Science, 6*, 214.
Leucker, M., Mahlein, A.-K., Steiner, U., & Oerke, E.-C. (2016). Improvement of lesion phenotyping in Cercospora beticola-sugar beet interaction by hyperspectral imaging. *Phytopathology, 106*, 177–184.
Leucker, M., Wahabzada, M., Kersting, K., Peter, M., Beyer, W., Steiner, U., et al. (2017). Hyperspectral imaging reveals the effect of sugar beet quantitative trait loci on cercospora leaf spot resistance. *Functional Plant Biology, 44*, 1–9.
Lemnatec. https://www.plant-phenomics.ac.uk/index.php/resources/ (Last accessed 7 October 2017).
Litwiller, D. (2005). Cmos vs. ccd: Maturing technologies, maturing markets-the factors determining which type of imager delivers better cost performance are becoming more refined. *Photonics Spectra, 39*, 54–61.

Liu, Z.-Y., Huang, J.-F., & Tao, R.-X. (2008). Characterizing and estimating fungal disease severity of rice brown spot with hyperspectral reflectance data. *Rice Science, 15*, 232–242.
Li, L., Zhang, Q., & Huang, D. (2014). A review of imaging techniques for plant phenotyping. *Sensors, 14*, 20078–20111.
Luo, J., Ying, K., & Bai, J. (2005). Savitzky–Golay smoothing and differentiation filter for even number data. *Signal Processing, 85*, 1429–1434.
Lu, S., Shimizu, Y., Ishii, J., Washitani, I., & Omasa, K. (2012). Detection of invasive plant with hyperspectral imagery in the riverbed of kinu river, Japan. In *Geoscience and remote sensing symposium (IGARSS), 2012 IEEE international* (pp. 4813–4816). IEEE.
Mahlein, A.-K. (2016). Plant disease detection by imaging sensors–parallels and specific demands for precision agriculture and plant phenotyping. *Plant Disease, 100*, 241–251.
Mahlein, A.-K., Hammersley, S., Oerke, E.-C., Dehne, H.-W., Goldbach, H., & Grieve, B. (2015). Supplemental blue led lighting array to improve the signal quality in hyperspectral imaging of plants. *Sensors, 15*, 12834–12840.
Mahlein, A.-K., Oerke, E.-C., Steiner, U., & Dehne, H.-W. (2012). Recent advances in sensing plant diseases for precision crop protection. *European Journal of Plant Pathology, 133*, 197–209.
Mahlein, A.-K., Rumpf, T., Welke, P., Dehne, H.-W., Plümer, L., Steiner, U., et al. (2013). Development of spectral indices for detecting and identifying plant diseases. *Remote Sensing of Environment, 128*, 21–30.
Mahlein, A.-K., Steiner, U., Dehne, H.-W., & Oerke, E.-C. (2010). Spectral signatures of sugar beet leaves for the detection and differentiation of diseases. *Precision Agriculture, 11*, 413–431.
Mahlein, A.-K., Steiner, U., Hillnhütter, C., Dehne, H.-W., & Oerke, E.-C. (2012). Hyperspectral imaging for small-scale analysis of symptoms caused by different sugar beet diseases. *Plant Methods, 8*, 1.
Malenovskỳ, Z., Turnbull, J. D., Lucieer, A., & Robinson, S. A. (2015). Antarctic moss stress assessment based on chlorophyll content and leaf density retrieved from imaging spectroscopy data. *New Phytologist, 208*, 608–624.
Matsuda, O., Tanaka, A., Fujita, T., & Iba, K. (2012). Hyperspectral imaging techniques for rapid identification of arabidopsis mutants with altered leaf pigment status. *Plant and Cell Physiology, 53*, 1154–1170.
Min, M., Lee, W. S., Burks, T. F., Jordan, J. D., Schumann, A. W., Schueller, J. K., et al. (2008). Design of a hyperspectral nitrogen sensing system for orange leaves. *Computers and Electronics in Agriculture, 63*, 215–226.
Mishra, P., Cordella, C. B., Rutledge, D. N., Barreiro, P., Roger, J. M., & Diezma, B. (2016). Application of independent components analysis with the {JADE} algorithm and {NIR} hyperspectral imaging for revealing food adulteration. *Journal of Food Engineering, 168*, 7–15.
Mishra, P., Herrero-Langreo, A., Barreiro, P., Roger, J., Diezma, B., Gorretta, N., et al. (2015). Detection and quantification of peanut traces in wheat flour by near infrared hyperspectral imaging spectroscopy using principal-component analysis. *Journal of Near Infrared Spectroscopy, 23*, 15–22.
Mo, C., Kim, M. S., Kim, G., Cheong, E. J., Yang, J., & Lim, J. (2015). Detecting drought stress in soybean plants using hyperspectral fluorescence imaging. *Journal of Biosystems Engineering, 40*, 335–344.
Mohd Shahrimie, M. A., Mishra, P., Mertens, S., Dhondt, S., Wuyts, N., & Scheunders, P. (2016). Modeling effects of illumination and plant geometry on leaf reflectance spectra in close-range hyperspectral imaging. In *WHISPERS - evolution in remote sensing* (pp. 1–4). IEEE.
Montes, J. M., Melchinger, A. E., & Reif, J. C. (2007). Novel throughput phenotyping platforms in plant genetic studies. *Trends in Plant Science, 12*, 433–436.
Mutka, A. M., & Bart, R. S. (2015). Image-based phenotyping of plant disease symptoms. *Frontiers in Plant Science, 5*.
Nicotra, A., Hofmann, M., Siebke, K., & Ball, M. (2003). Spatial patterning of pigmentation in evergreen leaves in response to freezing stress. *Plant, Cell & Environment, 26*, 1893–1904.
Ochoa, D., Cevallos, J., Vargas, G., Criollo, R., Romero, D., Castro, R., et al. (2016). Hyperspectral imaging system for disease scanning on banana plants. In *SPIE Commercial+ scientific sensing and imaging* (p. 98640M). International Society for Optics and Photonics.
Oerke, E.-C., Herzog, K., & Toepfer, R. (2016). Hyperspectral phenotyping of the reaction of grapevine genotypes to plasmopara viticola. *Journal of Experimental Botany, 67*, 5529–5543. arXiv http://jxb.oxfordjournals.org/content/67/18/5529.full.pdf+html.
Onoyama, H., Ryu, C., Suguri, M., & Iida, M. (2013). Potential of hyperspectral imaging for constructing a year-invariant model to estimate the nitrogen content of rice plants at the panicle initiation stage. In *IFAC Proceedings* (Vol. 46, pp. 219–224).
PHENOVISION. http://www.plant-phenotyping.org/phenovision. (Last accessed 7 October 2017).
PlantScreen. http://www.psi.cz/products/plantscreen. (Last accessed 7 October 2017).
Polder, G., & van der Heijden, G. (2010). Measuring ripening of tomatoes using imaging spectrometry. In *Hyperspectral imaging for food quality analysis and control* (pp. 369–402).
Posadas, B. B., Lee, W. S., Hong, Y., & Kim, S. (2015). Detecting marssonina blotch using hyperspectral imaging and hierarchical clustering. In *2015 ASABE annual international meeting* (p. 1). American Society of Agricultural and Biological Engineers.
Qin, J. (2010). Instruments for constructing hyperspectral imaging systems. In *Hyperspectral imaging for food quality analysis and control*. New York: Elsevier.
Rajendran, D. K., Park, E., Nagendran, R., Hung, N. B., Cho, B.-K., Kim, K.-H., et al. (2016). Visual analysis for detection and quantification of Pseudomonas cichorii disease severity in tomato plants. *The Plant Pathology Journal, 32*, 300.
Rascher, U., Blossfeld, S., Fiorani, F., Jahnke, S., Jansen, M., Kuhn, A. J., et al. (2011). Non-invasive approaches for phenotyping of enhanced performance traits in bean. *Functional Plant Biology, 38*, 968–983.
Rogass, C., Mielke, C., Scheffler, D., Boesche, N. K., Lausch, A., Lubitz, C., et al. (2014). Reduction of uncorrelated striping noise applications for hyperspectral pushbroom acquisitions. *Remote Sensing, 6*, 11082–11106.
Römer, C., Wahabzada, M., Ballvora, A., Pinto, F., Rossini, M., Panigada, C., et al. (2012). Early drought stress detection in cereals: Simplex volume maximisation for hyperspectral image analysis. *Functional Plant Biology, 39*, 878–890.
Roscher, R., Behmann, J., Mahlein, A.-K., Dupuis, J., Kuhlmann, H., & Plümer, L. (2016). Detection of disease symptoms on hyperspectral 3d plant models. In *ISPRS annals of photogrammetry, remote sensing and spatial information sciences* (pp. 89–96).
Rumpf, T., Mahlein, A.-K., Steiner, U., Oerke, E.-C., Dehne, H.-W., & Plümer, L. (2010). Early detection and classification of plant diseases with support vector machines based on hyperspectral reflectance. *Computers and Electronics in Agriculture, 74*, 91–99.
Saeys, Y., Inza, I., & Larrañaga, P. (2007). A review of feature selection techniques in bioinformatics. *Bioinformatics, 23*, 2507–2517.
Sankaran, S., Mishra, A., Ehsani, R., & Davis, C. (2010). A review of advanced techniques for detecting plant diseases. *Computers and Electronics in Agriculture, 72*, 1–13.
Savitzky, A., & Golay, M. J. (1964). Smoothing and differentiation of data by simplified least squares procedures. *Analytical Chemistry, 36*, 1627–1639.

Springob, K., Nakajima, J.-i., Yamazaki, M., & Saito, K. (2003). Recent advances in the biosynthesis and accumulation of anthocyanins. *Natural Product Reports, 20*, 288–303.
Sytar, O., Brestic, M., Zivcak, M., Olsovska, K., Kovar, M., Shao, H., et al. (2017). Applying hyperspectral imaging to explore natural plant diversity towards improving salt stress tolerance. *Science of the Total Environment, 578*, 90–99.
Tang, X., & Pearlman, W. A. (2006). Three-dimensional wavelet-based compression of hyperspectral images. In *Hyperspectral data compression* (pp. 273–308). Springer.
Tsai, F., Lin, E.-K., & Yoshino, K. (2007). Spectrally segmented principal component analysis of hyperspectral imagery for mapping invasive plant species. *International Journal of Remote Sensing, 28*, 1023–1039.
Ustin, S. L., & Gamon, J. A. (2010). Remote sensing of plant functional types. *New Phytologist, 186*, 795–816.
Varpe, A. B., Rajendra, Y. D., Vibhute, A. D., Gaikwad, S. V., & Kale, K. (2015). Identification of plant species using non-imaging hyperspectral data. In *2015 international conference on man and machine interfacing (MAMI)* (pp. 1–4). IEEE.
Vigneau, N., Ecarnot, M., Rabatel, G., & Roumet, P. (2011). Potential of field hyperspectral imaging as a non destructive method to assess leaf nitrogen content in wheat. *Field Crops Research, 122*, 25–31.
Wahabzada, M., Mahlein, A.-K., Bauckhage, C., Steiner, U., Oerke, E.-C., & Kersting, K. (2016). Plant phenotyping using probabilistic topic models: Uncovering the hyperspectral language of plants. *Scientific Reports*, 6.
Walter, A., Liebisch, F., & Hund, A. (2015). Plant phenotyping: From bean weighing to image analysis. *Plant Methods, 11*, 1.
Wu, D., & Sun, D.-W. (2013). Advanced applications of hyperspectral imaging technology for food quality and safety analysis and assessment: A review part i: Fundamentals. *Innovative Food Science & Emerging Technologies, 19*, 1–14.
Xiaobo, Z., Jiewen, Z., Holmes, M., Hanpin, M., Jiyong, S., Xiaopin, Y., et al. (2010). Independent component analysis in information extraction from visible/near-infrared hyperspectral imaging data of cucumber leaves. *Chemometrics and Intelligent Laboratory Systems, 104*, 265–270.
Xiaobo, Z., Jiyong, S., Limin, H., Jiewen, Z., Hanpin, M., Zhenwei, C., et al. (2011). In vivo noninvasive detection of chlorophyll distribution in cucumber (cucumis sativus) leaves by indices based on hyperspectral imaging. *Analytica Chimica Acta, 706*, 105–112.
Xie, C., Shao, Y., Li, X., & He, Y. (2015). Detection of early blight and late blight diseases on tomato leaves using hyperspectral imaging. *Scientific Reports*, 5.
Yeh, Y.-H., Chung, W.-C., Liao, J.-Y., Chung, C.-L., Kuo, Y.-F., & Lin, T.-T. (2016). Strawberry foliar anthracnose assessment by hyperspectral imaging. *Computers and Electronics in Agriculture, 122*, 1–9.
Yu, K.-Q., Zhao, Y.-R., Li, X.-L., Shao, Y.-N., Liu, F., & He, Y. (2014). Hyperspectral imaging for mapping of total nitrogen spatial distribution in pepper plant. *PLoS One, 9*, e116205.
Zhang, C., Liu, F., Kong, W., & He, Y. (2015). Application of visible and near-infrared hyperspectral imaging to determine soluble protein content in oilseed rape leaves. *Sensors, 15*, 16576–16588.
Zhu, H., Cen, H., Zhang, C., & He, Y. (2016). Early detection and classification of tobacco leaves inoculated with tobacco mosaic virus based on hyperspectral imaging technique. In *2016 ASABE annual international meeting* (p. 1). American Society of Agricultural and Biological Engineers.